agriculture

MDPI

Article

Effect of Vibration Conditions on the Seed Suction Performance of an Air-Suction Precision Seeder for Small Seeds

Yu Wang [1,2], Wenhang Zhang [1,2], Xiwen Luo [1,2], Ying Zang [1,2], Ligang Ma [1,2], Wenpeng Zhang [1,2], Jiahao Liu [1,2] and Shan Zeng [1,2,*]

[1] College of Engineering, South China Agricultural University, Guangzhou 510642, China; yu-wang@scau.edu.cn (Y.W.)
[2] Key Laboratory of Key Technology on Agricultural Machine and Equipment of the Ministry of Education, South China Agricultural University, Guangzhou 510642, China
* Correspondence: shanzeng@scau.edu.cn; Tel.: +86-020-38676975

Abstract: The air-suction precision seeder for small seeds is a planting machine, characterized by precision, high efficiency, and ease of operation, that uses air suction technology to sow small grain seeds at set intervals and depths into the soil. However, the forced vibration, enhanced by the increase in the operating speed, affects the seeding accuracy of the seeder and limits the seeding efficiency. To study the influence of vibration conditions on the seed suction performance of the air-suction precision seeder, we developed a computational fluid dynamics–discrete element coupling method to construct a bidirectional fluid–solid coupling numerical simulation model of the seed suction process under vibration conditions. Within the range of operating speeds from 0.6 km/h to 8 km/h, we quantitatively studied the population movement under different vibration frequencies, vibration amplitudes, negative pressure values, and seeding disc speeds and verified the simulation model and its analysis results through bench tests. The numerical results show that the interaction between the vibration frequency, vibration amplitude, and negative pressure value has the most significant impact on the single-seed rate. In addition, via variance analysis and response surface analysis, the optimal range of negative pressure values for achieving high single-seed rates under different vibration frequencies (4~10 Hz), vibration amplitudes (3~7.5 mm), and seeding disc speeds (4~50 rpm) was determined. The results indicate that, rather than the higher the negative pressure value, the higher the seed suction rate, the optimal negative pressure value for achieving a high seed suction rate varies with the specific vibration frequencies and amplitudes.

Keywords: air-suction precision seeder; vibration; small seeds; CFD–DEM coupling

check for updates

Citation: Wang, Y.; Zhang, W.; Luo, X.; Zang, Y.; Ma, L.; Zhang, W.; Liu, J.; Zeng, S. Effect of Vibration Conditions on the Seed Suction Performance of an Air-Suction Precision Seeder for Small Seeds. *Agriculture* **2024**, *14*, 559. https://doi.org/10.3390/agriculture14040559

Received: 22 February 2024
Revised: 21 March 2024
Accepted: 26 March 2024
Published: 1 April 2024

Copyright: © 2024 by the authors. Licensee MDPI, Basel, Switzerland. This article is an open access article distributed under the terms and conditions of the Creative Commons Attribution (CC BY) license (https://creativecommons.org/licenses/by/4.0/).

1. Introduction

Precision seeding refers to the process by which seeding machinery quantitatively places seeds in rows and holes in the field according to the planting requirements of crops, serving as a crucial means to improve the accuracy and efficiency of crop seeding [1,2]. The core component for achieving precision seeding is the precision seeder, whose efficiency and quality directly influence the subsequent growth and yield of crops [3,4]. Pneumatic precision seeders, developed from conventional mechanical precision seeders, represent advanced implements and include various types such as air-suction, air-blowing, and air-pressure mechanisms [5–7]. Among these seeders, air-suction precision seeders, relying on the adhesive action generated by negative pressure airflow to control the trajectory of seed movement, have become the main development direction of precision seeding machinery due to their less stringent requirements on seed size, low seed damage rates, and ease in achieving the quantitative hole-seeding requirement of one seed per hole [8].

The rapid and efficient development of modern agriculture poses new challenges for the operating speed of air-suction precision seeders. In comparison with the high-speed operation capabilities of air-suction precision seeders for large and medium-sized seeds

such as peanuts, corn, and rice [8], most small-seed crops such as vegetables, flowers, and grains face increased difficulty in precision seeding due to their light seed weight, small volume, and irregular shapes, leading to a decrease in the sensitivity of seed recognition by seeders [9]. Although pelletized seeds with spherical coatings have improved the adaptability of irregularly shaped small seeds to mechanical operations to some extent, seeds with diameters less than 3 mm still impose higher requirements on the structural design and operational parameter control of air-suction precision seeders.

As the operating speed of seeding machines in the field increases, the mechanical vibration of the seeding machine intensifies, drawing the attention of researchers to the impact of vibration characteristics on the performance of seeders. Wang et al. [10] conducted a vibration frequency analysis of mechanical corn precision seeders, indicating that, when the operating speed exceeds 5 km/h, the frequency distribution of the seeding machine's vibration energy is mainly low-frequency vibration, and the vibration intensity of the seeding machine increases as the operating speed increases but does not affect the frequency distribution of the vibration energy. For air-suction precision seeders, Zhang et al. [11] and Liu et al. [12] established dynamic simulation models of pneumatic precision seeders for corn and soybeans, respectively, studied the impact of the mechanical vibration of seeders on population movement, and optimized negative pressure values within a certain forward speed range in order to avoid the adverse effects of vibration on the seeding process. Existing research mainly focuses on large-seed seeders, no-tillage seeders, and precision seeding equipment for tray seedling cultivation, with relatively little research on precision seeders for small seeds. As the small size, light weight, and fragility of small seeds pose challenges to technical research on and the development of air-suction precision seeders, scholars [13–16] have mainly focused on factors such as the seeding disc speed, the negative pressure value, and suction hole geometry parameters affecting the seed suction performance of seeders. The working process of air-suction precision seeders can be divided into three main stages (filling, carrying, and releasing processes). Among these processes, the ability of the suction holes to achieve precise seed suction during the filling and carrying processes is the primary factor determining the uniformity and stability of seeding. Liao et al. [17], through vibration bench tests, verified that the vibration intensity and frequency are key factors affecting the filling and carrying processes, noting that low-frequency vibration significantly reduces the uniformity and stability of seed suction. Even though the existing research indicates that the increase in the mechanical vibration resulting from an increase in the operating speed is a key factor affecting the seeding performance of small seeders, there is still no relevant research elucidating the impact of vibration on the seed suction performance of precision seeders for small seeds.

To investigate the effects of vibration characteristics on the seed suction performance of precision seeders for small seeds, we studied the seed suction performance of the 2BSQ-10 air-suction precision seeder for small seeds under different vibration conditions. Based on computational fluid dynamics (CFD) and the discrete element method (DEM), a bidirectional CFD–DEM coupling numerical simulation model under vibration conditions was developed. The main parameters investigated included the vibration frequency, the vibration displacement amplitude, the seeding disc speed, and the negative pressure of the seeder. The vibration response characteristics of the seeder under high-speed seeding operations and the mechanism underlying their impact on the seed suction performance during the filling and carrying processes were studied quantitatively. Additionally, optimal negative pressure values for achieving high single-seed rates under different working conditions were obtained through variance analysis and response surface analysis, and the numerical results were validated through bench tests.

2. Structure and Working Principle of the Seeder

The 2BSQ-10 air-suction precision seeder for small seeds, developed by the scientific research team of the Key Laboratory of Agricultural Machinery and Equipment of the Ministry of Education, South China Agricultural University, adopts a circular disk circulation

method for negative pressure for filling and carrying processes and for positive pressure for the discharging process [18–21]. Its structure, as shown in Figure 1, includes such components as a base shell, a shaft, a seeding disc, and a seed box. The seeding chamber can be divided into three zones (a filling zone (I), a carrying zone (II), and a discharging zone (III)). The overall length of the seeder is 190 mm, the width is 80 mm, and the height is 250 mm. The diameter of the clock tray is 129 mm, the thickness is 3 mm, and there are a total of 20 seed suction holes. The seeder is connected to the frame through flange seats on the base shell using bolts. The seeding disc is driven to rotate by a sprocket wheel connected to the shaft, and seeds are supplied from the seed box through the seed inlet pipe into the filling zone.

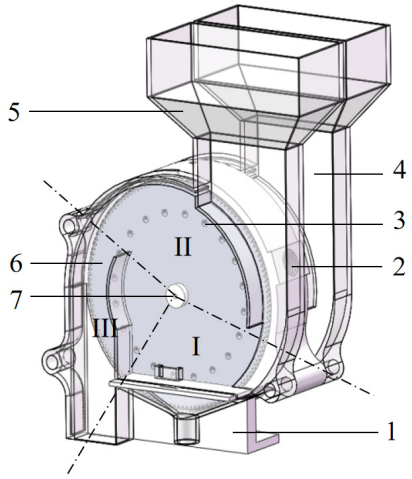

Figure 1. Structure of the air-suction precision seeder. 1, base shell; 2, suction port for the fan; 3, suction hole; 4, seed feed pipe; 5, seed box; 6, seeding disc; 7, shaft. Note: I, II, and III refer to the filling zone, carrying zone, and discharging zone, respectively.

During operation, seeds fall from the inlet pipe to the bottom of the planter and accumulate in the filling zone. The outlet of the negative pressure chamber is connected to a fan, generating negative pressure in the chamber. The seeding disc rotates counterclockwise at a uniform speed under the drive of the transmission shaft. Seeds in the filling zone are adsorbed into the suction holes at the other end of the seeding disc due to the negative pressure, thus rotating along with the seeding disc. The adsorbed seeds pass through the carrying zone to reach the discharging zone. At this point, the negative pressure chamber is blocked, and the seeding disc is connected to positive pressure. Seeds fall into the seed furrows under the action of positive pressure and gravity [22,23].

3. Numerical Simulation Model of Bidirectional Gas–Solid Coupling under Vibration Conditions

3.1. Bidirectional Gas–Solid Coupling Method

During the operation of the air-suction precision seeder, it is subjected to the combined effects of the airflow field, the particle field, and the gravitational field [24]. A bidirectional CFD–DEM gas–solid coupling method was adopted for the numerical simulation [25], which considers the interaction between particles and the airflow field, in order to analyze the motion of particles and the flow field. The effects of the fluid on particles include the drag force, the pressure gradient force, and the lift force. In the pneumatic planter, the main consideration is the drag force of the fluid on particles and the particles' gravity. The interaction of particles with the fluid was coupled by superimposing the volume force of particles within the fluid phase in the form of momentum exchange source terms [26].

The CFD–DEM bidirectional gas–solid coupling numerical simulation model was constructed using ANSYS Fluent 2023 R1 [27] and ANSYS Rocky 2023 R1 [28]. In each iteration step of the model, the flow field of the planting cavity is first calculated through

CFD. The drag force model is used to calculate the force exerted by the fluid on each particle. Then, the DEM calculates the displacement field of particles and updates the position, velocity, and other information of particles in the form of momentum sinks for the next iterative calculation. The DEM model of the air-suction precision seeder built in Rocky is shown in Figure 2a. The CFD model of the air-suction precision seeder built in Fluent is illustrated in Figure 2b, which includes the flow field in the negative pressure chamber, the seed box, and the suction holes.

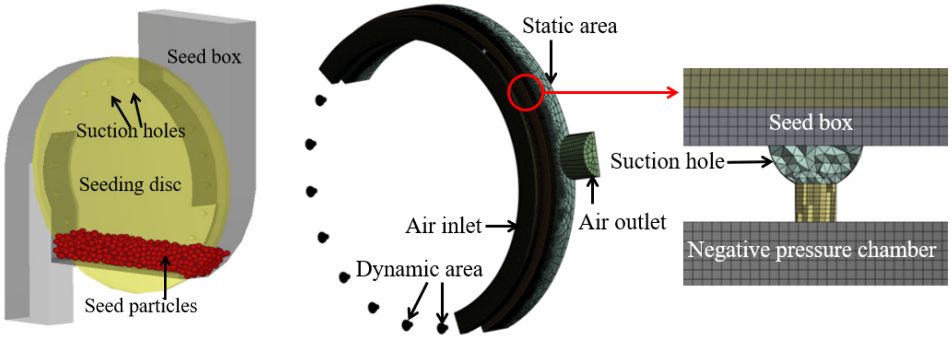

(**a**) DEM model (**b**) CFD model

Figure 2. CFD–DEM bidirectional gas–solid coupling numerical simulation model.

To accurately simulate the fluid flow state of the seeding hole, it is necessary to refine the mesh of the fluid domain of the seeding hole so that the mesh size of the seeding hole is not of the same order of magnitude as the characteristic size of particles. Since the particle volume is more than ten times the size of the grid cell, a semi-analytical method suitable for bidirectional coupling was selected. The negative pressure chamber and seed box adopted structured meshes (with the hexahedral mesh unit type, 230,377 elements, and 258,033 nodes), while the suction holes utilized a combination of structured and unstructured meshes (primarily hexahedral and tetrahedral meshes, 52,080 elements, and 15,620 nodes). Since the suction holes undergo circular motion relative to the seed box and negative pressure chamber, the corresponding sliding mesh motion was defined in Fluent, where the suction holes were designated as dynamic mesh regions and the seed box and negative pressure chamber regions were static mesh zones.

3.2. Simulation Parameter Settings

3.2.1. DEM Model Parameter Settings

Regarding the coupling method, the multiphase coupling method was chosen in Rocky for bidirectional coupling between particles and the fluid.

Regarding motion frames, in order to quantitatively study the impact of vibrations on the movement of seeds inside the seed box, in Rocky, the seed box and seeding disc models were described by motion frames, where the corresponding vibration frequency and amplitude were input in order to depict their vibration behavior. To depict the harmonic vibration characteristics, the motion velocity during vibration was defined as follows:

$$v(t) = 2\pi f D \cos(2\pi f t) \quad (1)$$

where $v(t)$ represents the vibration velocity in m/s, f denotes the vibration frequency in Hz, D is the vibration amplitude in mm, and t signifies the time in s.

Additionally, since the seeding disc rotates about its shaft while vibrating, an additional motion frame was required in order to input the corresponding rotation speed for its rotational behavior.

Regarding seed particles, granulated seeds of Xilan cabbage were selected to be the test samples for small-seed testing. The physical properties of granulated seeds depend on the coating material and processing techniques. The granulated seeds are spherical

after processing. The diameter of the seeds ranges from 2.3 to 3.3 mm, with approximately 65% distributed between 2.7 and 3.0 mm and approximately 80% distributed between 2.5 and 3.1 mm. Therefore, spherical particles with a diameter of 3 mm were simulated to represent granulated seeds. In Rocky, the constant adhesive force model was selected, in which the adhesive distance and force fraction were set to 0.1 mm and 0.4, respectively, and the rolling resistance model was set to the "Linear Spring Rolling Limit".

Regarding contact interaction, the seeding disc was made of stainless steel, the seed box was made of photosensitive resin, and the seed particles were granulated seeds with a density of 586.9 kg/m^3. The mechanical properties and physical characteristics of the seed particles, stainless steel, and photosensitive resin are shown in Table 1. Detailed descriptions of the physical properties of the seeds are provided in [29]. To govern the interaction between seed particles and the seeding disc, parameters such as the collision recovery coefficient, coefficient of static friction, and coefficient of dynamic friction were determined using calibration methods based on the angle of rest and the static friction coefficient.

Table 1. Physical parameters of the metering device and seed particles.

Materials	Seeds	Stainless Steel	Photosensitive Resin
Poisson's ratio	0.3	0.3	0.43
Modulus of elasticity/MPa	1.82×10	2.158×10^5	1.3×10^3
Density kg/m^3	1245	7890	1240
Collision recovery coefficient	0.35	0.55	0.242
Coefficient of static friction	0.1	0.35	0.3
Coefficient of dynamic friction	0.4	0.05	0.18

3.2.2. CFD Model Parameter Settings

Regarding the flow model, in order to coordinate with the coupling method set in Rocky, the Eulerian model was chosen in the multiphase flow model.

Regarding boundary conditions, the inlet was set to be a pressure inlet connected to atmospheric pressure, and the outlet was set to be a pressure outlet with the pressure value determined by the numerical value in the simulated orthogonal experimental design. To depict the vibration characteristics of the flow field model, the motion velocity was set to be the same as that of the seeding box and seeding disc.

Regarding the moving mesh, the moving mesh in Fluent was utilized to handle the vibration of the entire model and the rotation of the fluid domain in the suction holes.

The selection of the time step is crucial to the accuracy and stability of the simulation and to accurately capturing rapidly changing flows or time-dependent phenomena. Additionally, the choice of the time step may affect the convergence of the simulation. In order to simulate the seeding process of the seeder effectively and improve the convergence of the simulation, a time step size of 0.0001 was determined based on multiple simulation tests.

3.2.3. Selection of Experimental Parameters

Considering that the leakage of seeds due to the forced vibration can occur when the seeding machine operates at a speed of 5 km/h, the speed range of 0.6 km/h (the minimum stable working speed) to 8 km/h (a high-speed working condition) was chosen for the analysis. The corresponding seeding disc speeds (4 rpm and 50 rpm) were selected as the lower and upper limits, respectively.

The single-seed rate, as an indicator of the seed suction performance of the seeder, refers to the ratio of the number of single seeds adsorbed by the suction holes of the seeding disc to the total number of suction holes rotated when the seeding disc rotates through a certain number of turns. Static tests on the seed suction performance of the seeder indicated that, when the pressure in the negative pressure chamber was −800 Pa, the seeding holes of the seeding disc were barely able to adsorb seeds, but the single-seed rate was very low. When the pressure was −1000 Pa, the single-seed rate reached 100%, while at −3000 Pa, some suction holes experienced over-suction phenomena. Therefore,

−800 Pa and −3000 Pa were set as the upper and lower limits of the negative pressure chamber's pressure, respectively.

On sandy loam soil with a moisture content of 25%, vibration acceleration data on the seeder operating at speeds ranging from 0.6 km/h to 8 km/h were collected using a vibration test system (EDM-2000, Hangzhou Yiheng Technology Co., Ltd., Hangzhou, China) as shown in Figure 3. The vibration of the seeding machine during field operation is characterized by random vibration. Due to the adoption of a parallel four-bar mechanism for individual seeders, the vertical vibration during the forward movement of the seeding machine is the most significant, with vibration frequencies mainly ranging from 5 Hz to 9 Hz as depicted in Figure 4. It should be noted that, when the speed is 0 km/h, the vibration generated mainly comes from the vibration of the tractor's engine and fan. In this study, the selected range of vibration frequencies for the vertical vibration was from 4 Hz to 10 Hz. To obtain the vibration amplitudes of the seeder at different operation speeds as shown in Figure 5, the original data were filtered using the band-pass filter method in frequency domain filtering, and frequency domain integration was employed to integrate the filtered data. The average vibration amplitude at the minimum operating speed was 3.075 mm, while it was 7.499 mm at the maximum operating speed. Hence, 7.5 mm and 3 mm were set as the upper and lower limits of the vibration amplitude, respectively.

Figure 3. Structure of the air-suction precision seeder.

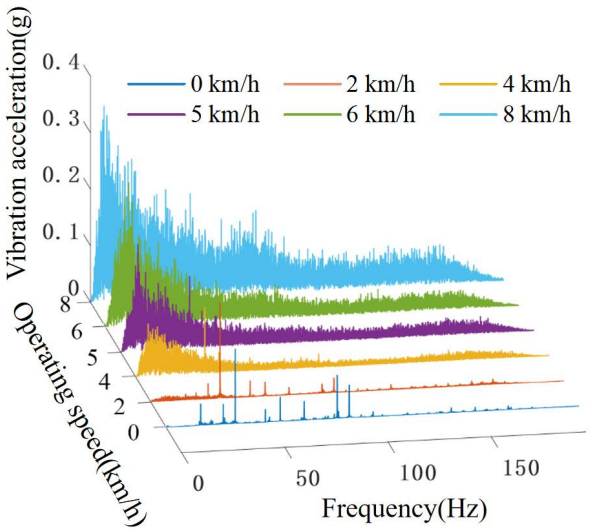

Figure 4. Vibration acceleration vs. frequency at different operating speeds.

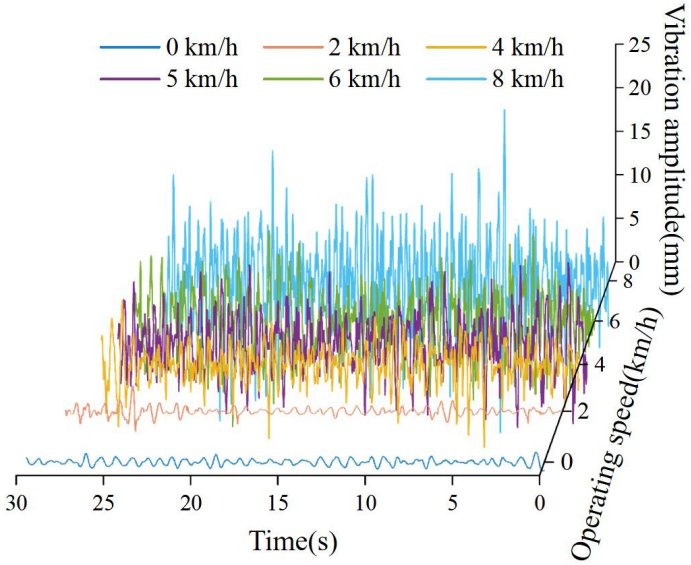

Figure 5. Vibration amplitude vs. time at different operating speeds.

3.3. Results and Validation of the Numerical Simulation

3.3.1. Results of the Numerical Simulation

The simulation results on the pressure contour in the negative pressure chamber during one vibration period are shown in Figure 6. Figure 6a–e show vibration equilibrium point 1, the vibration peak, vibration equilibrium point 2, the vibration valley, and vibration equilibrium point 3 within one vibration period. When the seed is adsorbed by the suction hole, the front part of the sinking ball of the seed suction hole will be blocked completely, so that the flow field in the negative pressure chamber will change. It can be seen from the change in the maximum negative pressure P_{max} and the minimum negative pressure P_{min} from the pressure contours that, when the seeder vibrates, the pressure field in the negative pressure chamber changes accordingly. The air outlet of the negative pressure chamber is close to the right end, and the flow velocity near the air outlet in the negative pressure chamber is higher, resulting in a higher absolute negative pressure value. The change in the pressure distribution is due to the fact that the seeding disc is constantly in a rotating state during the suction process, which causes the connection between the suction holes and the negative pressure chamber to be dynamically changed.

A seed particle adsorbed into a suction hole was selected in order to observe its speed change curve (Figure 7) during the carrying process of the seeder. From 0 to 0.64 s, the seed had not yet been adsorbed and mainly vibrated in the Y direction (i.e., the vertical direction) along with the seeder. Meanwhile, due to the interaction between seed particles and the friction between the seed particles and the seeding disc, the seed also exhibited small movements in the X and Z directions. At 0.64 s, the seed particle was adsorbed into the suction hole, causing a slight surge in its speed in all three directions. From 1.8 to 1.95 s, the seed detached from the suction hole and its speed gradually increased until it was discharged through the seed drop opening under the effect of gravity. Moreover, the absolute velocity and the velocity in the Y direction of the seed exhibited very similar patterns, indicating that the movement of the seed in the Y direction was the dominant component when the seeder was operating under vibration conditions.

A comparison of the absolute velocity curves of seeds in three adjacent suction holes during the carrying process of the seeder under vibration and non-vibration conditions is shown in Figure 8. It can be seen that the variations in the velocity of the three seeds in the adjacent suction holes are essentially the same. Under non-vibration conditions, the seeds do not exhibit periodic fluctuations, but the other trends in velocity changes are essentially consistent with those under vibration conditions.

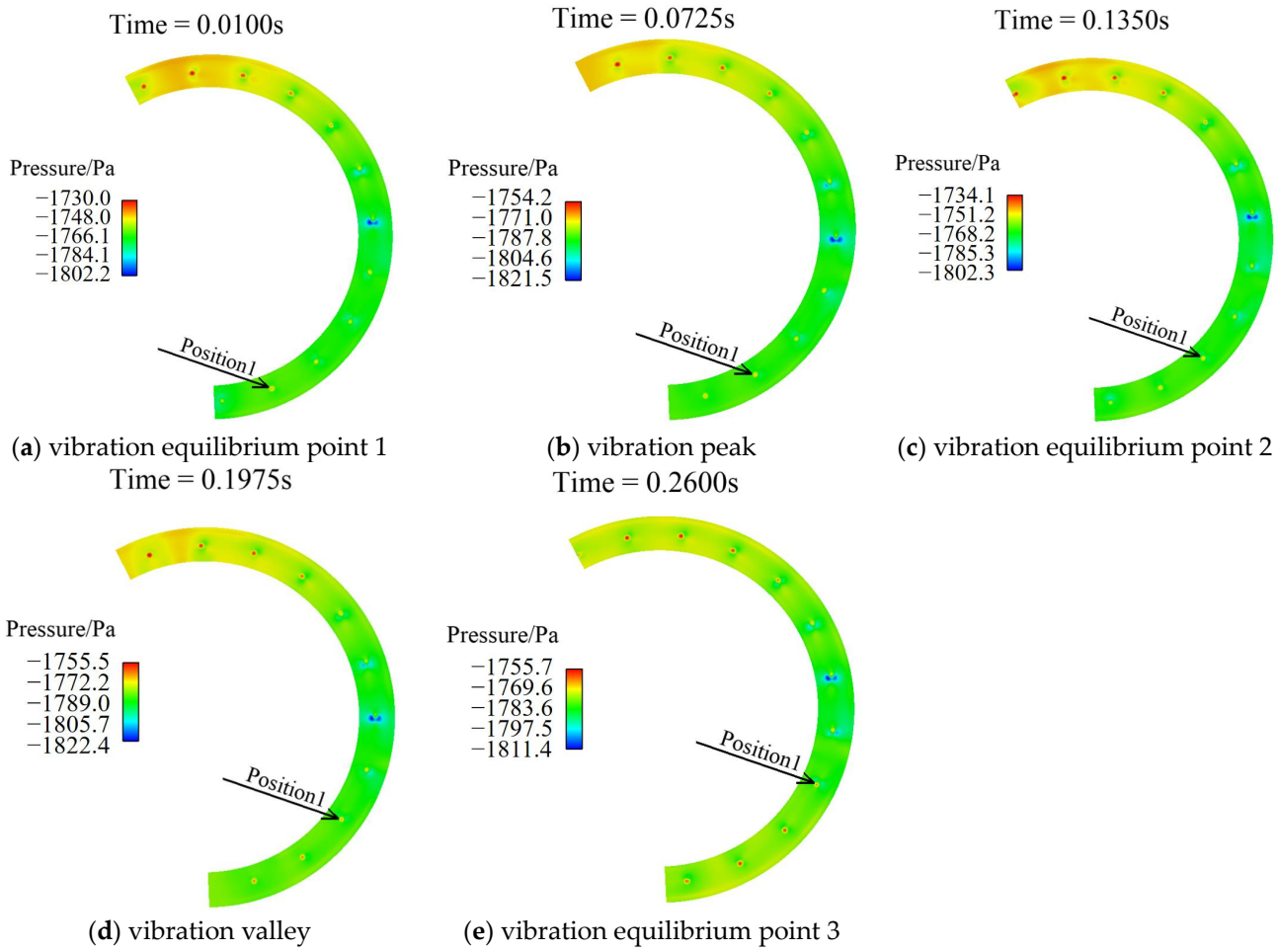

Figure 6. Pressure contours in the negative pressure chamber.

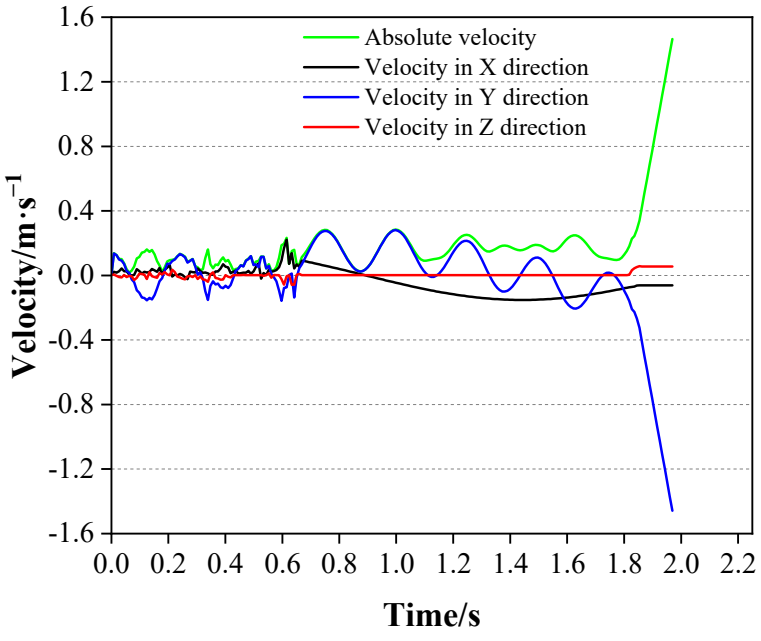

Figure 7. Velocity curves of the seed.

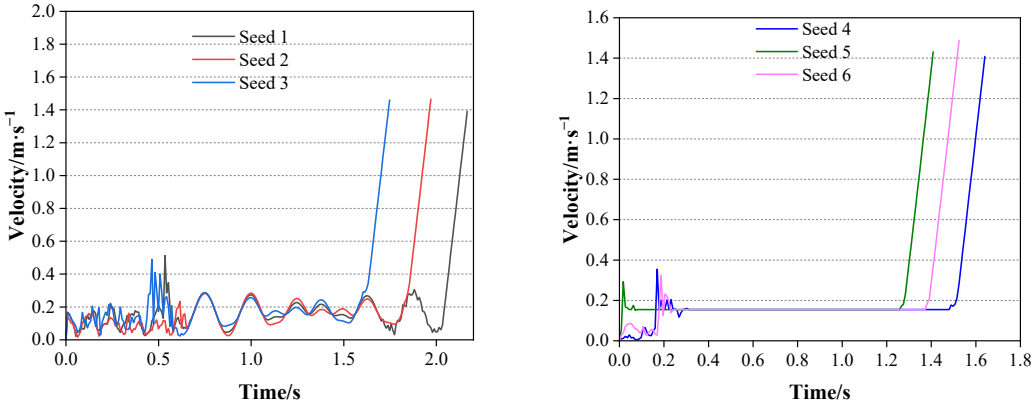

(**a**) vibration condition (**b**) non-vibration condition

Figure 8. Velocity curves of seeds under vibration conditions and non-vibration conditions.

3.3.2. Validation of the Numerical Simulation

The effectiveness of the CFD–DEM bidirectional gas–solid coupling numerical simulation model was validated through an experimental test on a vibration bench. The vibration apparatus (EDM-2000 electric vibration test system, Hangzhou Yiheng Technology Co., Ltd., Hangzhou, China) included a vibration cylinder, a vertical platform, a power amplifier, a fan, sensors, a vibration controller (MI-8008 24-channel, Hangzhou Yiheng Technology Co., Ltd., Hangzhou, China), and a computer as shown in Figure 9. Two different operating conditions with different vibration parameters were selected (Condition 1, vibration frequency, 5 Hz; vibration amplitude, 4.13 mm; seeding disc speed, 15 rpm; negative pressure value, −1350 Pa and Condition 2, vibration frequency, 8.5 Hz; vibration amplitude, 4.13 mm; seeding disc speed, 38 rpm; negative pressure value, −1350 Pa). The seed suction performance was recorded when the seeder was operating stably, and the results were evaluated based on the single-seed rate. The single-seed rate was determined as the ratio of the total number of single seeds adsorbed by all suction holes to the total number of suction holes every three revolutions of the seeding disc.

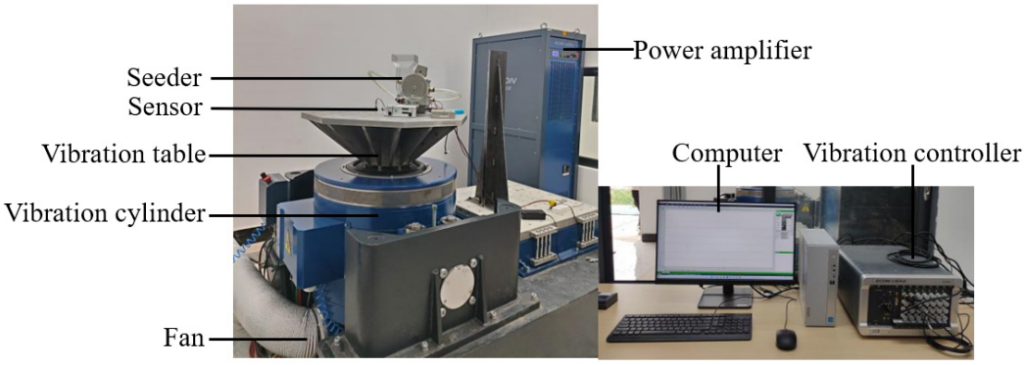

Figure 9. Vibration bench for seed suction performance under vibration conditions.

The seed suction performance in the numerical and bench tests is shown in Figure 10. A comparison of single-seed rates is given in Table 2, which indicates that the results of the simulation and experimental tests are generally consistent. The main source of error lies in the fact that the seeds in the experiment were not consistent in terms of quantity and size with the simulated particles.

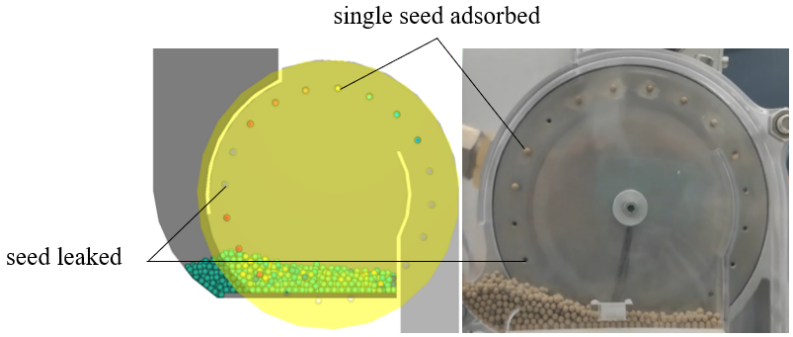

(**a**) Result of the numerical test (**b**) Result of the bench test

Figure 10. Seed suction performance in the numerical and bench tests.

Table 2. Comparison of results in the numerical and bench tests.

		Single-Seed Rate/%	Absolute Error/%
Working condition 1	Numerical test Bench test	90 91.7	1.7%
Working condition 2	Numerical test Bench test	65 73.3	8.3%

4. Effect of Vibration Conditions on Seed Suction Performance

4.1. Numerical Experiment Scheme

In order to study the filling and carrying processes of the seeder under vibration conditions, the CFD–DEM bidirectional gas–solid coupling numerical simulation model was used to perform a rotation orthogonal combination test. The vibration frequency, vibration amplitude, seeding disc speed, and negative pressure value of the seeder were used as the experimental factors X_1, X_2, X_3, and X_4, respectively. The single-seed rate was used as an evaluation indicator to establish a four-factor and five-level quadratic regression rotation orthogonal combination test. The zero-level value of each experimental factor was set. The star arms of the limit values of each factor were selected to be 2 and −2. The factor coding table is shown in Table 3. The quadratic regression rotation orthogonal combination test design was completed using Design-Expert 13 as shown in Table 4.

Table 3. Encoding of experimental factors.

Encoding Values	Test Factors			
	X_1 Vibration Frequency/Hz	X_2 Vibration Amplitude/mm	X_3 Seeding Disc Speed/rpm	X_4 Negative Pressure Absolute Value/Pa
2 (Asterisk arm)	10	7.5	50	3000
1	8.5	6.375	38.5	2450
0	7	5.25	27	1900
−1	5.5	4.125	15.5	1350
−2 (Asterisk arm)	4	3	4	800

Table 4. Experimental plan and results.

Test Number	Test Factors				Test Indicators
	X_1	X_2	X_3	X_4	Single-Seed Rate/%
1	−1	−1	−1	−1	89.45
2	1	−1	−1	−1	74.45
3	−1	1	−1	−1	89.45
4	1	1	−1	−1	69.45

Table 4. *Cont.*

Test Number	Test Factors				Test Indicators
	X_1	X_2	X_3	X_4	Single-Seed Rate/%
5	−1	−1	1	−1	89.45
6	1	−1	1	−1	64.45
7	−1	1	1	−1	94.45
8	1	1	1	−1	79.45
9	−1	−1	−1	1	99.45
10	1	−1	−1	1	94.45
11	−1	1	−1	1	79.45
12	1	1	−1	1	74.45
13	−1	−1	1	1	94.45
14	1	−1	1	1	89.45
15	−1	1	1	1	79.45
16	1	1	1	1	74.45
17	−2	0	0	0	99.45
18	2	0	0	0	79.45
19	0	−2	0	0	94.45
20	0	2	0	0	79.45
21	0	0	−2	0	99.45
22	0	0	2	0	79.45
23	0	0	0	−2	54.45
24	0	0	0	2	64.45
25	0	0	0	0	79.45
26	0	0	0	0	79.45
27	0	0	0	0	74.45
28	0	0	0	0	74.45
29	0	0	0	0	79.45
30	0	0	0	0	74.45
31	0	0	0	0	79.45

4.2. Results of the Numerical Experiment

Using Design-Expert 13, the results of the numerical experiment and the regression equation were analyzed by variance analysis and a significance test. As shown in Table 5, the fitness terms of models for the single-seed rate and leakage rate were extremely significant ($p < 0.01$), and the lack-of-fit terms were not significant, which fitted the actual situation well. After eliminating the insignificant regression terms, under the premise of ensuring that the regression model is significant and the lack-of-fit terms are not significant, the regression equations of the single-seed rate and leakage rate were as follows:

$$\begin{aligned} Y = {} & 77.86 - 5.63X_1 - 3.54X_2 - 1.88X_3 + 2.29X_4 + 3.43X_1X_4 + 2.19X_2X_3 \\ & -5.31X_2X_4 + 3.4X_1^2 + 2.78X_2^2 + 3.4X_3^2 - 4.1X_4^2 \end{aligned} \quad (2)$$

Table 5. ANOVA table of the single-seed rate.

Source of Variance	Test Factors			
	Sum of Squares	Degree of Freedom	F	*p*
Model	3452.1	14	16.67	<0.0001 **
X_1	759.38	14	51.35	<0.0001 **
X_2	301.04	1	20.36	0.0004 **
X_3	84.38	1	5.71	0.0296 *
X_4	126.04	1	8.52	0.0100 **
X_1X_2	1.56	1	0.1057	0.7494
X_1X_3	1.56	1	0.1057	0.7494
X_1X_4	189.06	1	12.78	0.0025 **
X_2X_3	76.56	1	5.18	0.0370 *
X_2X_4	451.56	1	30.54	<0.0001 **

Table 5. *Cont.*

Source of Variance	Test Factors			
	Sum of Squares	Degree of Freedom	F	*p*
X_3X_4	14.06	1	0.9509	0.3440
X_1^2	330.62	1	22.36	0.0002 **
X_2^2	220.25	1	14.89	0.0014 **
X_3^2	330.62	1	22.36	0.0002 **
X_4^2	480.62	1	32.5	<0.0001 **
Residual error	236.61	1		
Lack of fit	193.75	16	2.71	0.1172
Error	42.86	10		
Total	3688.71	6		
R^2				0.9359
R^2_{Adj}				0.8797
R^2_{pred}				0.6816

** indicates a highly significant term ($p < 0.01$); * indicates a significant term ($p < 0.05$).

By fixing the two factors other than the analyzed factors at the zero level, the interaction between the remaining two factors on the single-seed rate can be analyzed. The effects of the vibration frequency, vibration amplitude, seeding disc speed, and negative pressure on the single-seed rate were obtained, and their response surface plots are shown in Figure 11a–f.

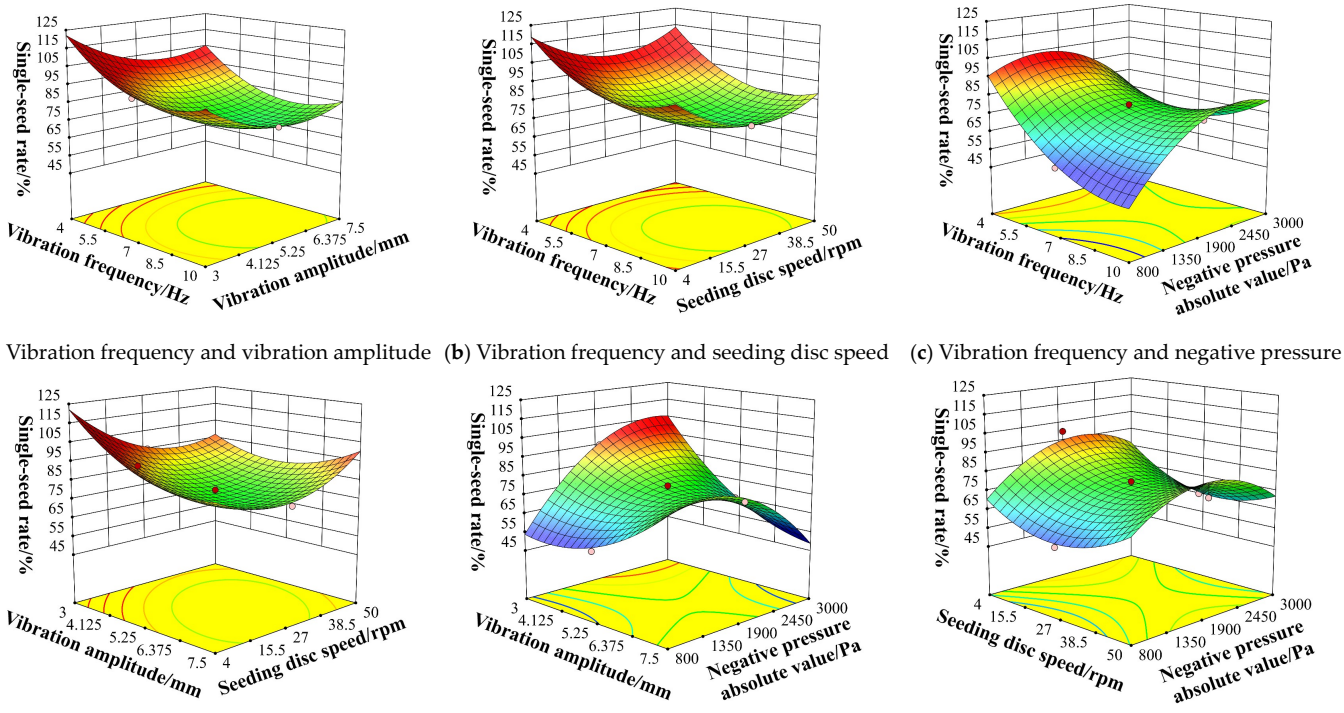

(**a**) Vibration frequency and vibration amplitude (**b**) Vibration frequency and seeding disc speed (**c**) Vibration frequency and negative pressure

(**d**) Vibration amplitude and seeding disc speed (**e**) Vibration amplitude and negative pressure (**f**) Seeding disc speed and negative pressure

Figure 11. The impact of interaction factors on single-seed rate.

From Figure 11c, it can be seen that, when the negative pressure is −800~−1000 Pa, as the vibration frequency increases the single-seed rate gradually decreases. When the negative pressure is −1000~−3000 Pa, as the vibration frequency increases the single-seed rate first decreases and then increases. When the vibration frequency is 4~9 Hz, as the negative pressure increases the single-seed rate first increases and then decreases. When the vibration frequency is 9~10 Hz, as the negative pressure increases the single-seed rate gradually increases.

From Figure 11e, it can be seen that, when the negative pressure is −800~−1100 Pa, as the vibration amplitude increases the single-seed rate gradually increases. When the negative pressure is −1100~−2400 Pa, as the amplitude increases the single-seed rate first decreases and then increases. When the negative pressure is −2400~−3000 Pa, as the vibration amplitude increases the single-seed rate gradually decreases. When the vibration amplitude is 3~3.75 mm, as the negative pressure increases the single-seed rate gradually increases. When the vibration amplitude is 3.75~7.5 mm, as the negative pressure increases the single-seed rate first increases and then decreases.

The response surface plots in Figure 11c and e have a high degree of inclination and a steep slope ($p < 0.01$), indicating that the interaction between the vibration frequency and the negative pressure and the interaction between the vibration amplitude and the negative pressure have a significant impact on the single-seed rate.

From Figure 11d, it can be seen that, when the seeding disc speed is 4–9 rpm, as the vibration amplitude increases the single-seed rate gradually decreases. When the seeding disc speed is 9–50 rpm, as the vibration amplitude increases the single-seed rate first decreases and then increases. When the vibration amplitude is any value between 3 and 7.5 mm, as the seeding disc speed increases the single-seed rate first decreases and then increases. The response surface plot has a high degree of inclination and a steep slope and the contour plot is elliptic ($p < 0.05$), indicating that the interaction between the vibration amplitude and the seeding disc speed has a significant impact on the single-seed rate.

From Figure 11a,b,f, it can be seen that, for the interactions between the 4~10 Hz vibration frequency and the 3~7.5 mm vibration amplitude, the 4~10 Hz vibration frequency and the 4~50 rpm seeding disc speed, and the 4~50 rpm seeding disc speed and the −800~−3000 Pa negative pressure, when one factor remains unchanged, as another factor increases, the single-seed rate has the same change, namely it first decreases and then increases or first increases and then decreases. The response surface plot has a low degree of inclination and a gentle slope and the contour plot is nearly circular ($p > 0.05$), indicating that the interaction between the vibration frequency and the vibration amplitude, the vibration frequency and the seeding disc speed, and the seeding disc speed and the negative pressure has no significant impact on the single-seed rate.

Through the above analysis, it was found that the seed suction performance is affected by multiple factors and their interactions. Among these interactions, the interaction between the vibration frequency, vibration amplitude, and negative pressure is the most significant. Although the seeding disc speed has a greater impact on the single-seed rate, it has a smaller impact on the optimal negative pressure range. In order to determine the optimal negative pressure range for achieving high single-seed rates under different vibration frequencies, vibration amplitudes, and seeding disc speeds, further analysis was conducted on the data shown in Figure 11c,e. The results of the analysis of different vibration conditions corresponding to the optimal negative pressure ranges are summarized in Table 6.

Table 6. Optimal negative pressure ranges for different working conditions.

Vibration Frequency/Hz	Vibration Amplitude/mm	Negative Pressure Absolute Value/Pa
4–6	3–4.5	−1900~−2100/−2400~−2600
	4.5–6	−1500~−1700
	6–7.5	−900~−1100/−1200~−1400
6–8	3–4.5	−2400~−2700
	4.5–6	−1700~−1900/−2100~−2300
	6–7.5	−1300~−1500/−1800~−2000
8–10	3–4.5	−2700~−3000
	4.5–6	−2100~−2300/−2300~−2800
	6–7.5	−1500~−1700/−2200~−2400

4.3. Verification of Numerical Results

Four working conditions were randomly selected to verify the numerical analysis results via bench tests, and each working condition was tested under four negative pressure conditions (−900 Pa, −1600 Pa, −2300 Pa, and −3000 Pa). The numerical analysis results and bench test results were compared. During the test, after the seeder stabilized the seed suction, the single-seed rate was counted every three revolutions of the seeding disc. The bench test results and the comparison with the numerical test results are given in Table 7. It can be seen that the numerical analysis results are basically consistent with the best negative pressure value ranges of the bench tests and simulation tests, which verifies the reliability of the numerical analysis results.

Table 7. Bench test results and a comparison with numerical test results.

Working Condition	Vibration Frequency/Hz	Vibration Amplitude/mm	Speed of Seeding Disc/rpm	Negative Pressure Value/Pa	Single-Seed Rate/%	Optimal Negative Pressure Value in the Numerical Test/Pa
1	5	5	6.23	−900	61.67%	−1500~−1700
	5	5	6.23	−1600	95.00%	
	5	5	6.23	−2300	95.00%	
	5	5	6.23	−3000	95.00%	
2	5	5	12.5	−900	92.50%	−1500~−1700
	5	5	12.5	−1600	95.00%	
	5	5	12.5	−2300	95.00%	
	5	5	12.5	−3000	90.00%	
3	9	7	6.23	−900	97.50%	−1500~−1700 −2200~−2400
	9	7	6.23	−1600	100.00%	
	9	7	6.23	−2300	100.00%	
	9	7	6.23	−3000	92.50%	
4	9	7	50	−900	63.33%	−1500~−1700 −2200~−2400
	9	7	50	−1600	81.67%	
	9	7	50	−2300	85.00%	
	9	7	50	−3000	90.00%	

It can be noticed from Condition 2 that the higher the negative pressure value the higher the single-seed rate. The results on Condition 4 show that, under some vibration conditions, it is difficult to achieve a 100% single-seed rate, but we can still obtain higher seed suction performance by adjusting the negative pressure value.

5. Conclusions

In this paper, a bidirectional fluid–solid coupling numerical simulation model of the filling and carrying processes of an air-suction precision seeder under vibration conditions was constructed using the CFD–DEM coupling method. Within the working speed range of 0.6 km/h to 8 km/h, quadratic regression rotation orthogonal combination tests were carried out to quantitatively study the seed suction performance of the seeder under different vibration frequencies, vibration amplitudes, negative pressure values, and seeding plate rotation speeds. Through variance analysis and response surface analysis of the results of the numerical experiment, it was found that that the interaction between the vibration frequency and the negative pressure and the interaction between the vibration amplitude and the negative pressure had a significant impact on the single-seed rate. The interaction between the vibration amplitude and the rotation speed of the seeding disc also had a significant impact on the single-seed rate. In addition, the optimal negative pressure value ranges for achieving a high single-seed rate were determined for different vibration and working conditions.

The CFD–DEM bidirectional fluid–solid coupling numerical simulation model that was constructed for the seed suction process of the seeder provides a feasible quantitative analysis approach to studying the influence of operating conditions and parameters on the working performance of air-suction precision seeders. The numerical analysis results could

help us optimize the operating parameters of precision seeders for small seeds and develop precision seeders with adaptive control of operating parameters.

Author Contributions: Conceptualization, Y.W. and S.Z.; methodology, Y.W.; software, W.Z. (Wenhang Zhang); formal analysis, L.M., W.Z. (Wenpeng Zhang) and J.L.; resources, Y.Z.; writing—original draft preparation, Y.W. and W.Z. (Wenhang Zhang); writing—review and editing, Y.W. and S.Z.; supervision, X.L. All authors have read and agreed to the published version of the manuscript.

Funding: The authors gratefully acknowledge the support provided by the National Key Research and Development Program of China (Grant No. 2021YFD2000403), the National Natural Science Foundation of China (Grant No. 32372002), the Central Guiding Local Science and Technology Development Project (Guike ZY22096023), and the Guangdong Province Rural Revitalization Strategy Special Project (Yue Cai Nong [2021] No. 170).

Institutional Review Board Statement: "Not applicable" for studies not involving humans or animals.

Data Availability Statement: The data that support the findings of this study are available from the corresponding author upon reasonable request.

Conflicts of Interest: The authors declare no conflicts of interest.

References

1. Cisternas, I.; Velásquez, I.; Caro, A.; Rodríguez, A. Systematic literature review of implementations of precision agriculture. *Comput. Electron. Agric.* **2020**, *176*, 105626. [CrossRef]
2. Luo, X.; Liao, J.; Zang, Y.; Ou, Y.; Wang, P. Developing from Mechanized to Smart Agricultural Production in China. *Strateg. Study CAE* **2022**, *24*, 46–54. [CrossRef]
3. Lai, Q.; Jia, G.; Su, W.; Hong, F.; Zhao, J. Design and test of ginseng precision special-hole type seed-metering device with convex hull. *Trans. Chin. Soc. Agric. Mach.* **2020**, *51*, 60–71. [CrossRef]
4. Hu, H.; Zhou, Z.; Wu, W.; Yang, W.; Li, T.; Chang, C.; Ren, W.; Lei, X. Distribution characteristics and parameter optimisation of an air-assisted centralised seed-metering device for rapeseed using a CFD-DEM coupled simulation. *Biosyst. Eng.* **2021**, *208*, 246–259. [CrossRef]
5. Gao, X.; Xie, G.; Li, J.; Shi, G.; Lai, Q.; Huang, Y. Design and validation of a centrifugal variable-diameter pneumatic high-speed precision seed-metering device for maize. *Biosyst. Eng.* **2023**, *227*, 161–181. [CrossRef]
6. Hu, M.; Xia, J.; Zhen, K.; Du, J.; Liu, Z.; Zhou, M. Design and experiment of inside-filling pneumatic high-speed precision seed-metering device for cotton. *Trans. Chin. Soc. Agric. Mach.* **2021**, *52*, 73–85. [CrossRef]
7. Han, D.; Zhang, D.; Jing, H.; Yang, L.; Cui, T.; Ding, Y.; Wang, Z.; Wang, Y.; Zhang, T. DEM-CFD coupling simulation and optimization of an inside-filling air-blowing maize precision seed-metering device. *Comput. Electron. Agric.* **2018**, *150*, 426–438. [CrossRef]
8. Yang, L.; He, X.; Cui, T.; Zhang, D.; Shi, S.; Zhang, R.; Wang, M. Development of mechatronic driving system for seed meters equipped on conventional precision corn planter. *Int. J. Agric. Biol. Eng.* **2015**, *8*, 1–9. [CrossRef]
9. Ding, Y.; Wang, K.; Liu, X.; Liu, W.; Chen, L.; Liu, W.; Du, C. Research progress of seeding detection technology for medium and small-size seeds. *Trans. CSAE* **2021**, *37*, 30–41. [CrossRef]
10. Wang, Q.; Zhu, L.; Li, M.; Huang, D.; Jia, H.; Zhuang, J. Vibration characteristics of corn no-tillage finger-type precision planter and its effect on seeding performance. *Trans. CSAE* **2019**, *35*, 9–18. [CrossRef]
11. Zhang, T.; Liu, F.; Zhao, M.; Liu, Y.; Li, F.; Chen, C.; Zhang, Y. Movement law of maize population in seed room of seed metering device based on discrete element method. *Trans. CSAE* **2016**, *32*, 27–35. [CrossRef]
12. Liu, Y.Q. Study on Vibration Characteristics of Air Suction No-Tillage Planter and Its Effect on Seed Metering Performance. Ph.D. Thesis, Inner Mongolia Agricultural University, Hohhot, China, 2017.
13. Zeng, S.; Wen, Z.; Liu, W.; Xu, Z.; He, S.; Wang, P. Optimal design and experiment of air-suction precision hole sowing seed metering device for small-grain vegetable seed. *J. South China Agric. Univ.* **2021**, *42*, 52–59. [CrossRef]
14. Gao, L.; Shi, B.; Liao, Q.; Zhang, B.; Zheng, J.; Liao, Y. Seeding performance of conical-hole seeding plate of the positive and negative pressure combination precision seed metering device for rapeseed. *Trans. Chin. Soc. Agric. Eng. (Trans. CSAE)* **2022**, *38*, 22–33. [CrossRef]
15. Wang, H.; Sun, X.; Chen, X.; Li, H.; Wang, Y. Design and test of air suction precision seed metering device for Brassica Chinensis. *J. Chin. Agric. Mech.* **2022**, *43*, 51–57. [CrossRef]
16. Pareek, C.M.; Tewari, V.K.; Machavaram, R. Multi-objective optimization of seeding performance of a pneumatic precision seed metering device using integrated ANN-MOPSO approach. *Eng. Appl. Artif. Intell.* **2023**, *117*, 105559. [CrossRef]
17. Liao, Y.; Qi, T.; Liao, Q.; Zeng, R.; Li, C.; Gao, L. Vibration characteristics of pneumatic combined precision rapeseed seeder and its effect on seeding performance. *J. Jilin Univ. (Eng. Technol. Ed.)* **2022**, *2*, 1184–1196. [CrossRef]
18. Tian, B.; Liao, Q.; Huang, H.; Shu, C.; Duan, H.; Li, J. Design of 2BFQ-6 Device of Combined Precision Rapeseed Seeder. *Trans. Chin. Soc. Agric. Mach.* **2008**, *39*, 211–213.

19. Li, M.; Liu, X.; Liao, Y.; Li, X. Pneumatic Cylinder-type Centralized Precision Metering Device for Rapeseed. *Trans. Chin. Soc. Agric. Mach.* **2013**, *44*, 68–73. [CrossRef]
20. Li, Y.; Wei, L.; Li, Q. Design and test of an inside-filling pneumatic precision centralized seed-metering device for rapeseed. *Int. J. Agric. Biol. Eng.* **2017**, *10*, 56–62. [CrossRef]
21. Yan, Q.; Liao, Y.; Liao, Q. Design and function analysis of dual-purpose rape-wheat pneumatic double-row metering device. *J. Huazhong Agric. Univ.* **2014**, *33*, 109–114. [CrossRef]
22. Motani, R.; Ji, C.; Tomita, T.; Kelley, N.; Maxwell, E.; Jiang, D.; Sander, M. Absence of Suction Feeding Ichthyosaurs and Its Implications for Triassic Mesopelagic Paleoecology. *PLoS ONE* **2013**, *8*, e66075. [CrossRef] [PubMed]
23. Liao, Q.; Li, J.; Tan, G. Experiment of Pneumatic Precision Metering Device for Rapeseed. *Trans. Chin. Soc. Agric. Mach.* **2009**, *40*, 44–48.
24. Li, Y.; Zhao, Z.; Chen, J.; Xu, L. Element Method Simulation of Seeds Motion in Vibrated Bed of Precision Vacuum Seeder. *Trans. Chin. Soc. Agric. Mach.* **2009**, *40*, 56–59.
25. Zhang, H.; Zhang, C.; Li, Z.; Ding, L.; Zhu, C.; Zhang, J. Simulation Analysis and Optimization of Vibration Characteristics of Corn Finger Clip Seeding Device Based on EDEM-RecurDyn Coupling. *Trans. Chin. Soc. Agric. Mach.* **2023**, *54*, 36–46. [CrossRef]
26. Han, D.; Zhang, D.; Yang, L.; Li, K.; Zhang, T.; Wang, Y.; Cui, T. EDEM-CFD simulation and experiment of working performance of inside-filling air-blowing seed metering device in maize. *Trans. Chin. Soc. Agric. Eng.* **2017**, *33*, 23–31. [CrossRef]
27. Fluent Inc. *Fluent CFD Software User Guide, Version 18.2*; Fluent Inc.: Lebanon, New Hampshire, 2023.
28. Rocky Development Team. *Rocky CFD Software User Manual, Version 3.5*; Ansys Inc.: Houston, TX, USA, 2023.
29. Yang, L.; Wang, Y.F. Calibration of Parameters of Coated Carrot Seeds Required in Discrete Element Method Simulation Based on Repose Angle of Particle Heap. *J. Agric. Mech. Res.* **2023**, *45*, 143–150. [CrossRef]

Disclaimer/Publisher's Note: The statements, opinions and data contained in all publications are solely those of the individual author(s) and contributor(s) and not of MDPI and/or the editor(s). MDPI and/or the editor(s) disclaim responsibility for any injury to people or property resulting from any ideas, methods, instructions or products referred to in the content.